ACS OMEGA

http://pubs.acs.org/journal/acsodf

Article

Superficial and Inkjet Scalable Printed Sensors Integrated with Iron Oxide and Reduced Graphene Oxide for Sensitive Voltammetric Determination of Lurasidone

Samar Y. Al-nami, Ali Q. Alorabi, Zehbah A. Al-Ahmed, Amal T. Mogharbel, Hana M. Abumelha, Mohammed A. Hussein,* and Nashwa M. El-Metwaly*

Cite This: *ACS Omega* 2023, 8, 10449−10458

Read Online

ACCESS | Metrics & More | Article Recommendations | Supporting Information

ABSTRACT: The present work demonstrated the fabrication and the electrochemical characterization of novel printed electrochemical sensors integrated with an innovative nanosensing platform based on the synergic electrocatalytic effect of iron oxide nanoparticles (FeONPs) and reduced graphene oxide (rGO) for precise voltammetric determination of the antipsychotic drug lurasidone hydrochloride (LUH). The features of the electrode surface fabricated using the ordinary inkjet printer were characterized by scanning electron microscopy and electrochemical impedance spectroscopy. Among different ink formulations, integration of the printing ink with the ratio 15 mg FeONPs and 20 mg rGO was found to be the most appropriate for sensitive quantification of LUH in biological fluids and pharmaceutical formulations in the presence of LUH degradation products. Under the optimized experimental and electroanalytical parameters, the recorded square-wave voltammograms were correlated to LUH within the linear concentration ranging from 50 to 2150 ng mL^{-1} with detection limit and limit of quantification values of 15.64 and 47.39 ng mL^{-1}, respectively. Based on the cyclic voltammograms recorded for LUH at different scan rates, the electrode reaction was assumed to be a diffusion reaction mechanism accompanied by the transfer of two electrons/protons through the oxidation of the five-membered ring nitrogen atom as assumed by the molecular orbital calculations carried out on the LUH molecule. The C_{max} of LUH and the efficiency of the fabricated sensors enabled their clinical application for monitoring LUH in human biological fluids and pharmaceutical formulations in the presence of degradants for diverse quality control applications and green chemistry analysis.

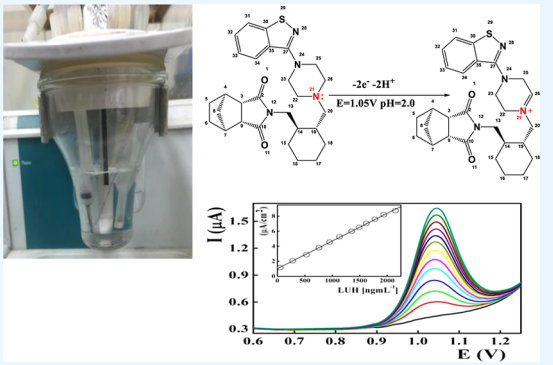

1. INTRODUCTION

Lurasidone hydrochloride (LUH) is one of the common drugs for treatment of bipolar disorder among other antipsychotic drugs for schizophrenia and marketed under the trade name Latuda.[1−3] In bipolar disorder, LUH can be administered with a mood stabilizer, e.g., valproate. The common side effects involve drowsiness, nausea, diarrhea, and movement disorders.[4] Other severe critical side effects include late movement disorder dysfunction, high blood sugar levels, angioedema, raised risk of suicide, and the neuroleptic malignant syndrome.[5,6]

Owing to high chemical stability, a noticeable low biodegradation rate, and a high toxicity level, quantification of LUH represents a crucial issue.[7,8] LUH is not official in any pharmacopeia, and surveying up to date has revealed the spectrophotometric[9−11] and chromatographic methods[12−16] as the common approaches for monitoring LUH residues in biological and pharmaceutical samples. Furthermore, the aforementioned techniques were reported to be time-consuming with multiple pretreatment steps, employing expensive operational instruments and solvents; therefore, they are not suitable for routine analysis and in situ measurements.[17] Introducing new pharmaceutical formulations represents a new challenge for their quantification and validation, and there is a continuous demand for the development of reliable, precise, sensitive, and selective analytical approaches for the detection and validation of newly approved medicines in their pharmaceutical dosage forms and biological fluids.

Electroanalytical approaches with the aid of tailor-made sensors have been proven to be an excellent choice for monitoring pharmaceutical compounds in biological and pharmaceutical samples.[18−21] In comparison to other techniques, electroanalytical methods showed significant advantages

Received: January 3, 2023
Accepted: February 27, 2023
Published: March 9, 2023

such as good reusability, excellent selectivity, and flexibility.[22,23] With their improved performance, electroanalytical approaches can be combined with other spectrometric and chromatographic techniques for monitoring pharmaceutical residues in biological and pharmaceutical samples. Carbonaceous-based electrodes represent a major category of the voltammetric working electrodes.[24−30] For biomedical and healthcare monitoring, the well-known glassy carbon and carbon paste electrodes are too bulky to be applied with the necessity for sterilization and regeneration which oppose the commercialization of such sensors. Therefore, introduction of disposable electrochemical printed sensors with their miniaturized planner structure is welcomed. Growing interest is reported for electroanalytical applications of the printed disposable sensors based on their mass production with a high degree of precision, accuracy, and excellent reproducibility.[31−38]

While developing a novel voltammetric sensor, investigations were carried out to improve the sensor performance through integration of the electrode matrix with various carbonaceous and metal/metal oxide nanostructures.[39−44] The electrocatalytic activity of the nanostructured materials and their ability to catalyze the electrode process enhance the kinetics of the electron-transfer process at the electrode surface, which in turn improves the electrode performance.

Fortification of the working electrode matrix with different metal oxide nanostructures is characterized by the strong adhesion of the metallic nanostructure to the graphite substrate, offering a stable electrocatalytic effect of the metallic centers. Iron oxide nanoparticles (FeONPs) represent one of the most popular electrode modifiers with a high electrocatalytic effect based on their band gaps and overall redox potentials.[45−49]

To the best of our knowledge, no electroanalytical approach has been reported for assaying LUH, and the electrochemical analysis of LUH with printed sensors integrated with FeONPs and reduced graphene oxide (rGO) is presented for the first time. The simple and reproducible mass production of the disposable carbon-based sensors represents the promising future of the present work. The impact of the electrode modifier, pH of the supporting electrolyte, variation of the scan rate, and other measuring parameters was evaluated. The reported sensors showed low detection limits with a prolonged operational lifetime.

2. EXPERIMENTAL SECTION

2.1. Reference Drug and Reagents. The standard LUH fresh solution was prepared by dissolving the appropriate amount of LUH standard material (3*a*,4,7,7*a*)-2-{(1,2)-2-[4-(1,2-benzisothiazol-3-yl)piperazin-1-ylmethyl] cyclohexyl methyl]hexahydro-4,7-methano-2-isoindole-1,3-dione, $C_{28}H_{37}ClN_4O_2S$, 529.18 g mol^{-1}) in demineralized water and kept at 4 °C.

Graphite carbon powder (1.0−2.0 μm, Aldrich), reduced graphene nanopowder (rGO), and iron oxide nanopowder (<50 nm, Sigma-Aldrich) were used for the preparation of the printing ink. Ink binders including carboxymethyl cellulose, isopropyl alcohol, and polyvinyl-pyrrolidone were analytical grade reagents. Universal Britton−Robinson (BR) buffer covering the pH range from 2 to 8 was prepared where the desired pH value was adjusted with NaOH solution.

2.2. Apparatuses. A Metrohm voltammetric analyzer (797 VA, Metrohm, Switzerland) was used for voltammetric measurements. The electrochemical cell was composed of a Ag/AgCl double-junction reference electrode, a platinum wire auxiliary electrode, and the printed sensor as working electrode (Figure S1). For the electrochemical characterization and screening of the tested nanomaterials, cyclic voltammetry (CV) and electrochemical impedance spectroscopy (EIS) were performed in ferricyanide (FCN) as the standard redox probe. A scanning electron microscope (S-4800, Hitachi Transport Co., Ltd., Japan) was used to investigate the precise morphology of the inkjet-printed electrodes.

2.3. Fabrication of rGO/FeONPs-Functionalized Printed Sensors. Printing ink with the desired formulation composed of 465 mg of synthetic graphite powder, 15 mL of isopropyl alcohol, and 5 mL of polyvinylpyrrolidone (10%) was mixed thoroughly with 200 mg of carboxymethyl cellulose in 40 mL of deionized water. The produced matrix was sonicated for 2 h and centrifuged at 5000 rpm for 30 min to assure its homogeneity. The produced ink was integrated with different ratios of FeONPs and rGO as follows: matrix I (0, 0), II (25 mg FeONPs, 10 mg rGO), III (20 mg FeONPs, 15 mg rGO), IV (15 mg FeONPs, 20 mg rGO), and finally matrix V (10 mg FeONPs, 25 mg rGO). After continuous stirring for 10 min, the mixture was further sonicated for 15 min to achieve complete homogeneity. The conductivity of the printing inks with different formulations was tested using a multimeter (Jenway 4510 Conductivity/TDS Meter) and found to be 220, 198, 165, 142, and 158 μS for matrices I to V, respectively. Furthermore, the viscosity of the produced ink matrix was measured using a NETZSCH rheometer, and the viscosity values ranged from 10 to 15 cps. The homemade FeONPs/rGO/graphite ink showed decent stability at room temperature for 30 days.

An Epson Eco-Tank L3160 Inkjet printer with a Micro Piezo print head, nozzle configuration: 180 Nozzles Black, minimum droplet size (3pl) with 5760 × 1440 DPI resolution (Epson Co., Ltd., China) was used for printing of the sensors on transparent overhead projector polyvinyl chloride (PVC) sheets (Figure S1). The ink cartridge was washed with water and ethanol, and 20 mL of the aforementioned ink matrices were transferred into the Eco-Tank System, and the electrodes, with dimensions 20 × 3 mm, were printed on the PVC sheets producing uniform quality and smooth lines. The printed flexible sensors were cured at 80 °C for 20 min, and their conductivities ranged from 8 to 10 kΩ/sq.

2.4. Analytical Procedures. The supporting electrolyte at pH 2 was fortified with different aliquots of the fresh LUH stock solution, and square-wave voltammograms were recorded at the optimal measuring parameters: voltage step, 6 mV; amplitude, 20 mV; frequency, 50 Hz; and scan rate, 0.2975 V. Calibration graphs were illustrated by plotting the current density against the LUH concentration.

2.5. Pharmaceutical and Biological Samples. Five tablets of the commercial Latuda pharmaceutical sample (assigned to contain 20 mg of lurasidone HCl, Sunovion Company) were weighed, crushed, and an amount equivalent to one tablet was dissolved in 50 mL of demineralized water. The drug solution was sonicated for 20 min at room temperature and filtered. Aliquots of the sample solution were analyzed following the voltammetric procedures in comparison with the chromatographic approach.[50]

Urine samples fortified with LUH standard solution were mixed with methanol, centrifuged to remove the protein, and

https://doi.org/10.1021/acsomega.3c00040
ACS Omega 2023, 8, 10449−10458

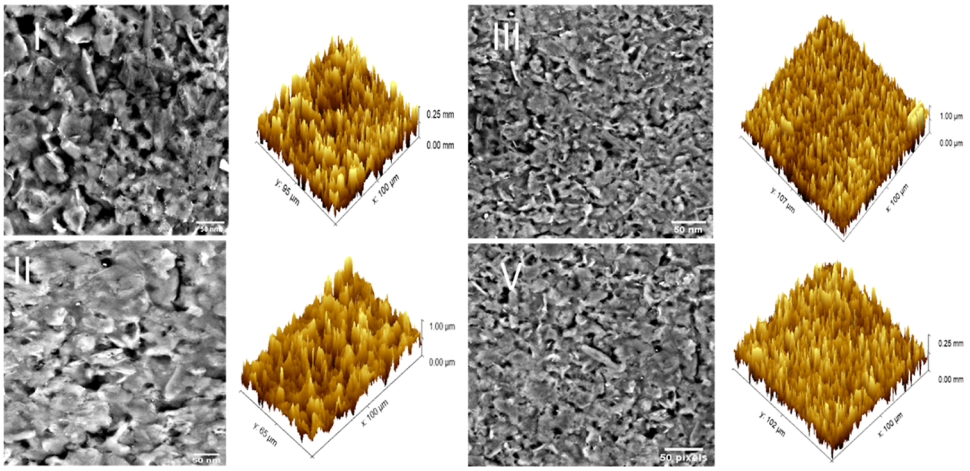

Figure 1. Morphological characteristics of FeONPs/rGO printed sensors (I−V) through SEM and AFM images.

the LUH content in the clear solution was tested voltammetrically in comparison with the chromatographic method.

2.6. Forced Degradation of LUH. The hydrolytic degradation of the LUH compound was carried out by dissolving 50 mg of the LUH standard sample in 50 mL of 2×10^{-1} mol L^{-1} NaOH or HCl under reflux at 130 °C for 3 h, where the progress of the LUH degradation was followed spectrophotometrically at 230 nm.[10] After cooling, the resultant degradant solutions were neutralized, and the volume was completed to the mark with water.

For oxidative degradation, 20 mg of standard LUH sample was dissolved in 10 mL of 10% H_2O_2 solution and incubated overnight at 50 °C. The final required concentration was made up by serial dilution with demineralized water, and voltammograms were recorded to check the interference from the degradation products.

2.7. Computational Calculations. Molecular orbital calculations by different Hukel, MM94, and MOPAC models were performed to confirm the proposed LUH redox mechanism at the FeONPs/rGO-functionalized electrode surface. Such estimations were performed with Gaussian ChemOffice 2017 suite programs.[51,52]

3. RESULTS AND DISCUSSION

3.1. Characterization of the Printed Electrode. *3.1.1. Morphological Studies.* The surface morphology of the carbon printed sensors functionalized with different ratios of rGO and FeONPs was evaluated by performing scanning electron microscopy (SEM) and atomic force microscopic studies on different regions of the electrode surface (Figure 1). SEM images of the electrodes reveal a highly porous and rough surface with a large number of small particles distributed throughout. The particles are typically in the range of 10−50 nm in size and are composed of iron oxide nanocrystals. The nanocrystals are arranged in an ordered array, with each particle having a distinct shape and size. The particles are interconnected by thin layers of metal oxides, which form a network that helps to increase the surface area available for electrochemical reactions.[53−56] Moreover, the nano iron oxide-modified screen-printed electrodes have a high degree of porosity, which increases their reactivity and enables them to be used for electrochemical sensing applications. The pores on the surface provide pathways for ions to move through, allowing for efficient electrochemical reactions to take place. Additionally, the porous nature of these electrodes allows them to absorb more electrolyte solution than conventional electrodes, resulting in improved performance. AFM can be used to measure the topography of the electrode surface, providing information on its roughness, grain size, and other features. The AFM images of nano iron oxide-modified screen-printed electrodes show a homogeneous distribution of nanoparticles at the electrode surface with an average particle size of around 20 nm. The particles are well-dispersed and have a uniform shape and size. The surface morphology is also characterized by a high degree of porosity, with many small pores visible in the AFM images. The AFM images also reveal that there is no significant agglomeration or clustering of nanoparticles on the electrode surface, indicating good dispersion and adhesion properties. Overall, these results indicate that nano iron oxide-modified screen-printed electrodes have a highly uniform and porous surface morphology which is suitable for electrochemical applications.

3.1.2. Electrochemical Characterization. In the present study, potassium ferricyanide $[K_3Fe(CN)_6]$ was selected as the redox couple system to estimate the electroactive surface area of the printed sensors through recording successive cyclic voltammograms at different scan rates ranged from 0.1 to 0.55 V s^{-1}, following the Randles−Sevcik equation.[57] As illustrated in Figure S2, well-defined reversible redox peaks (anodic and cathodic peaks) were recorded for ferricyanide/ferricyanide,[58] where the difference from the anodic peak to the cathodic peak ranged from 90 to 110 mV, and the ratio relationship of the anodic or cathodic peak current of (I_{pc}/I_{pa}) was in the range from 0.99 to 1.10. The relationship between the anodic or cathodic peak current versus the square root of the scan rate ($\upsilon^{1/2}$) can be expressed by the equation[59]

$$I_{pa} = (2.69 \times 10^5) A n^{3/2} {D_R}^{1/2} C_0 \nu^{1/2}$$

where I_{pa} refers to the anodic peak current, A is the surface area of the electrode, D_R is diffusion coefficient, ν is the scan rate, n is the number of electrons transferred, and C_0 is the concentration of $K_3Fe(CN)_6$. Thus, the estimated electroactive areas of FeONPs/rGO printed sensors (I−V) were 0.014, 0.02, 0.023, 0.028, and 0.024 cm^2, respectively. The highest electroactive surface area was recorded for electrode (IV) with the printing ink integrated with 15 mg of FeONPs and 20 mg of rGO. Moreover, ratios between the electrochemical surface area (ESA) or effective area (A_{eff}) and the

https://doi.org/10.1021/acsomega.3c00040
ACS Omega 2023, 8, 10449−10458

geometric area (Ag) were calculated to be R_f = 3.5:1, 5:1, 5.75:1, 7:1, and 6:1 for the aforementioned sensors in the same order.

EIS has been used to scrutinize the electron charge-transfer resistance and exchanges between the electrode surface and electrolyte solution (Figure 2). The estimated R_{ct} values were

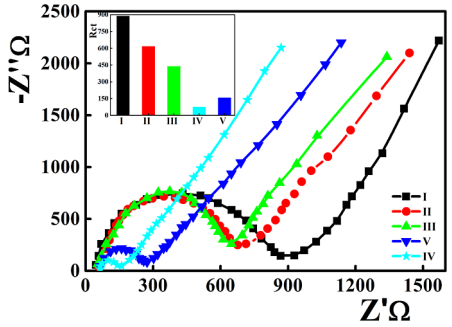

Figure 2. EIS for the printed sensors modified with different rGO/FeO ratios in 5.0 × 10^{-3} mol L^{-1} $[Fe(CN)_6]^{-3/-4}$/1.0 × 10^{-1} mol L^{-1} KCl solution.

889, 617, 438, 75.75, and 157.6 Ω corresponding to the sensors from I to V, respectively. Among the printed sensors, electrode (IV) exhibited the lowest R_{ct} value, suggesting its excellent electrical conductivity and surface wettability and exhibiting its optimized electrocatalytic activity. Based on the obtained R_{ct} values, the standard heterogeneous electron-transfer rate constant (k^0) of various modified electrodes was calculated using the following equation

$$k^0 = \frac{RT}{n^2AF^2R_{ct}C}$$

where n, T, R, F, and C represent the number of electrons, temperature (298 K), gas constant, Faraday constant, and concentration of the FCN solution, respectively (5.0 × 10^{-3} mol L^{-1} $K_3Fe(CN)_6^{-3/-4}$). The calculated k^0 value for the printed sensors integrated with FeONPs/rGO nanostructures were 4.03 × 10^{-6}, 2.15 × 10^{-6}, 3.11 × 10^{-6}, 1.08 × 10^{-6}, and 2.18 × 10^{-6} cm s^{-1}, respectively. These findings indicate that the proposed composite has greater conductivity, excellent electron transferability, and superior electrocatalytic activity among other electrodes.

3.2. Electrochemical Behavior of LUH. To explore the electrochemical behavior of the LUH molecule at the fabricated FeONPs/rGO printed sensors, cyclic voltammograms were recorded in BR buffer at pH 2.0 as illustrated in Figure 3a. On the unmodified graphite printed sensors, the LUH molecule exhibited a broad single irreversible anodic oxidation peak at 0.970 V. Upon fortification of the electrode matrix with FeONPs/rGO nanostructures, more than 10-fold amplification of the peak current was recorded, which may be attributed to the electrocatalytic effect of the fortified nanostructure toward the oxidation of LUH at the electrode surface in addition to the enhancement of the electroactive surface area of the electrode surface which facilitates the electron-transfer process. Gradual improvement of the peak height was monitored to reach its maximum performance on applying the electrode IV with the matrix composition 15 mg FeONPs and 20 mg of rGO (Figure 3b).

3.3. pH Effect on the Voltammetric Behavior of LUH. One of the crucial points for studying the electrochemical behavior of any oxidizable organic compound is the selection of the optimum pH value at which the oxidation peak reaches its maximum current value. Lurasidone hydrochloride showed two pK_a values at 1.96 and 8.50; therefore, its electrochemical behavior will be influenced by the pH value of the supporting electrolyte. For this investigation, cyclic voltammograms for LUH were recorded at various pH values ranging from 2.0 to 8.0 (Figure 4a). Within the pH range 2−3, LUH exhibited a well-defined single anodic peak which was further split into two peaks at a higher pH value (4−5). At lower pH values (<4), the LUH molecule mainly presents as a protonated form and provides the ionic bond N^+−H, while at higher pH values (>6.0), LUH exists as a deprotonated form. Thus, at pH 4−5, both forms are present, resulting in splitting of the oxidation peak.[60] The highest peak current was recorded at pH 2, which was around the pK_{a1} of the LUH molecule.

Additionally, negative shift of the peak potential was monitored by increasing the pH value of the supporting electrolyte (Figure 4b), postulating the involvement of the hydrogen proton in the oxidation of the LUH molecule at the electrode surface.[61,62] A linear relationship was illustrated between the oxidation peak potential and the pH value of the

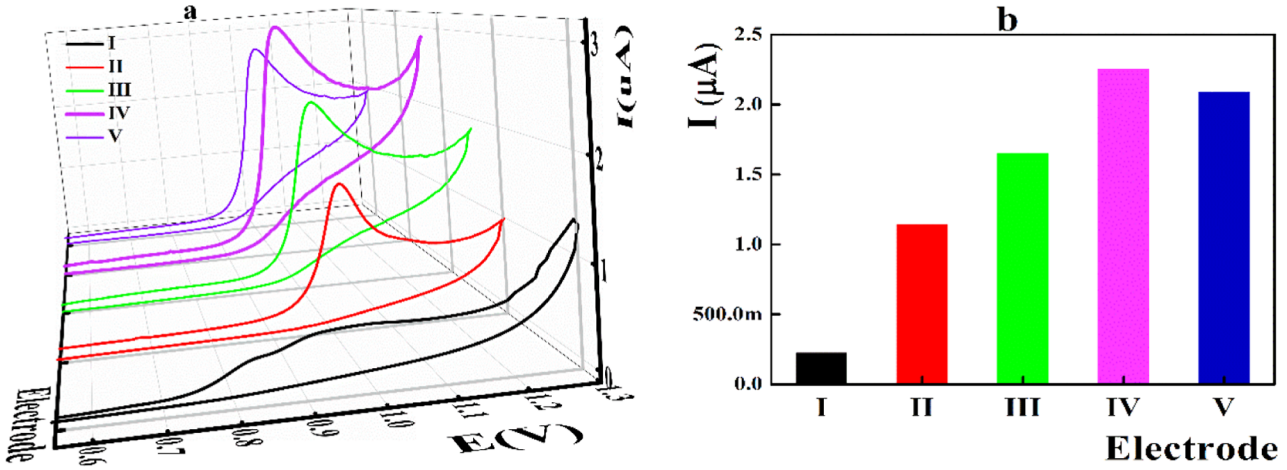

Figure 3. (a) Cyclic voltammograms recorded in the presence of 0.5 μg mL^{-1} LUH at FeONPs/rGO printed sensors and (b) peak height at different nanocomposite contents. Scan rate 100 mV s^{-1} at pH 2.

https://doi.org/10.1021/acsomega.3c00040
ACS Omega 2023, 8, 10449−10458

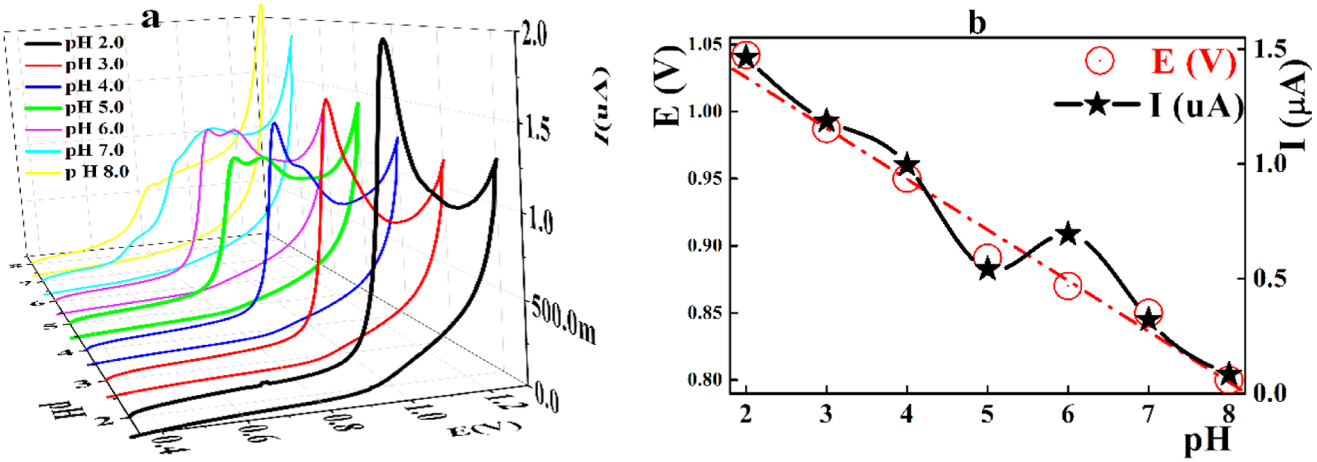

Figure 4. (a) Voltammetric behavior of 0.5 μg mL^{-1} LUH recorded at different pH values performed at FeONPs/rGO electrode (IV) and (b) peak currents and peak potentials recorded at different pH values. Scan rate was 100 mV s^{-1}.

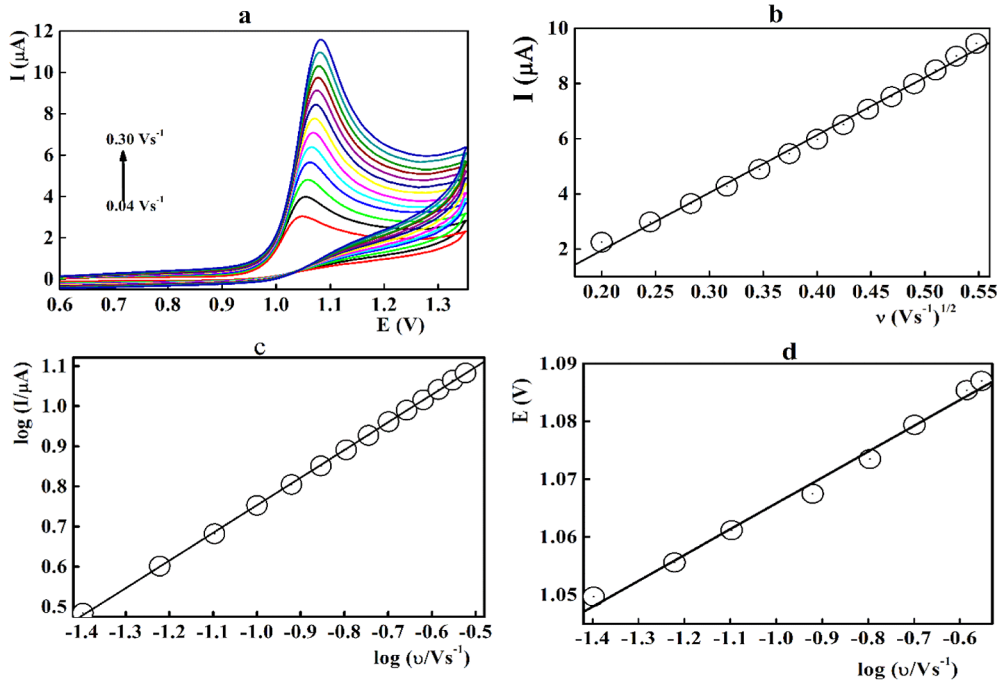

Figure 5. (a) Cyclic voltammograms for 0.5 μg mL^{-1} LUH at FeONPs/rGO printed sensors recorded at different sweep rates, (b) peak current against the square root of the scan rate, (c) log (I) of the peak current against log value of the scan rate, and (d) peak potential against log value of the scan rate.

supporting electrolyte [$E_{(V)} = -0.041$ [pH] + 1.1; $r^2 = 0.9909$]. The low value of the intercept indicates that there are no side reactions accompanying the oxidation of the LUH molecule, while the near Nernstian slope value assumes that equal number of electrons and protons are involved in the electrooxidation of the LUH molecule.[63,64]

3.4. Electrochemical Behavior at Different Scan Rate Values. The kinetics of the electrode reaction was studied through recording the successive cyclic voltammograms at different scan rates. As illustrated in Figure 5a, CVs were scanned at different scan rate values ranged from 0.040 to 0.300 V s^{-1}. Shifting of the peak potential to a more positive value with gradual improvement of the peak height was observed at higher scan rates. Additionally, an appropriately low background current was noticed at the electrode surface which may be explained on the basis of low interfacial capacitance.

Figure 5b illustrates the linear relationship between the anodic peak currents and the square root of the scan rate (I_p (A) = $-2.22 \times 10^{-6} + 2.08 \times 10^{-5}\ \nu^{1/2}$, $r^2 = 0.9980$). The high correlation coefficient indicates the irreversibility of the reaction at the electrode surface. Moreover, the relationship between the logarithm value of the redox peak current (log I) against the logarithm value of the scan rate (Figure 5c) shows that a near theoretical slope value of 0.553 was estimated, indicating that the redox process of the LUH molecule transfer to the electrode surface followed a diffusion-controlled reaction.[62,63,65]

Moreover, the peak potentials recorded at different scan rates showed a linear relationship against logarithmic values of the sweep rate ($E_{(V)} = 0.555 + 0.0445 \log \upsilon$; $r = 0.9871$, Figure

https://doi.org/10.1021/acsomega.3c00040
ACS Omega 2023, 8, 10449−10458

5d), suggesting the participation of 2.456 electrons (≈2) in the oxidation of the LUH molecule at the electrode surface.[66] Alternately, for irreversible reactions, the number of electrons that participated in the electrode reaction can be estimated based on the Nicholson and Schein equation[67]

$$\Delta E_p(\mathrm{mV}) = E_p - E_{p/2} = (47.7/\alpha n)$$

where ΔE_p is the potential difference, α is the charge-transfer coefficient, and n is the number of electrons. Consequently, the computed value αn was equal to 1.09, and in the case of irreversible voltammetric processes, α was considered to be equal to 0.5; thus the number of electrons transported in LUH oxidation was calculated as 2.18 (≈2).

3.5. Mechanism. Ultimately, to support the postulated oxidation mechanism of the LUH molecule at the electrode surface, the Chem office-17 theoretical simulation software was used.[51,52] Thus, the proposed mechanism for the irreversible electrochemical oxidation of LUH involves the transfer of two electrons and two protons based on the scan rate studies and pH effect and was confirmed by molecular orbital calculations (Table S1, Figure S6). The high-electron-density amine nitrogen group (with IUPAC count no. 21) in the aliphatic piperazine ring was oxidized through two-electron transfer and liberation of two protons (Scheme 1).[68]

Scheme 1. Computed Systematic Proposed Electrooxidation of LUH at the Electrode Surface

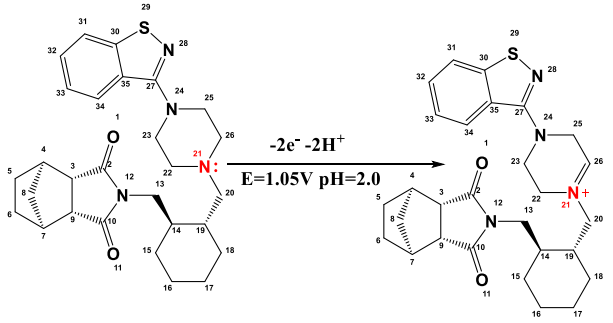

3.6. Validation of the LUH Sensor. The electroanalytical parameters for the square-wave voltammetry (SWV) measurements such as voltage step and pulse amplitude were optimized to achieve the highest performance (Figures S4 and S5). Based on the achieved results, the optimal measuring parameters were as follows: voltage step 6 mV, amplitude 20 mV, frequency 50 Hz, and scan rate 0.2975 V.

Under the optimized analytical experimental condition, the performance characteristics of the printed graphite sensors integrated with FeONPs/rGO nanoparticles were evaluated based on the ICH guidelines.[69] Different ascending increments of the LUH stock solution were added to the supporting electrolytes at pH 2, square-wave voltammograms were recorded, and the estimated peak heights were plotted against LUH concentration in a nanogram range (Figure 6 & Table 1). The limit of detection (LOD) and limit of quantification (LOQ) were estimated as LOD equal to 3.3 × (SD/S) and LOQ equal to 10 × (SD/S), where SD is the standard deviation of the intercept, and S is the slope of the calibration curves (n = 14) The corresponding LOD and LOQ values were 15.64 and 47.9 ng mL^{-1}, respectively.

The accuracy and precision were assessed using three different LUH concentrations: 550, 950, and 1600 ng mL^{-1}

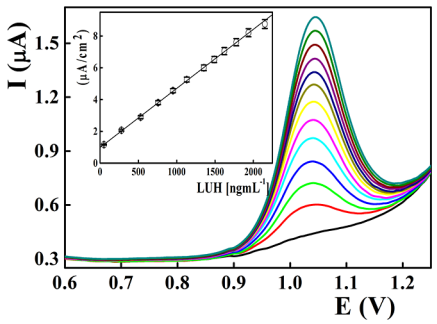

Figure 6. Square-wave voltammograms for different LUH concentrations recorded at FeONPs/rGO printed sensors in BR buffer pH 2.

Table 1. Analytical Performance and Linear Regression Curve of the Square-Wave Voltammograms Recorded at Different LUH Concentrations at FeONPs/rGO Printed Sensors[a]

parameters	
optimal pH value	2.0
peak potential	1.02 V
linearity range (ng mL^{-1})	50−2150
slope (μA mL^{-1}ng^{-1})	0.0096
SD of slope (μA mL^{-1}ng^{-1})	0.001
intercept (μA cm^{-2})	1.02
SD of intercept (μA cm^{-2})	0.0458
correlation coefficient (r)	0.9999
precision (% RSD)	
repeatability	0.86
intermediate precision	1.17
LOD (ng mL^{-1})	15.64
LOQ (ng mL^{-1})	47.9

[a] n = mean of five determinations. n = 13.

(Table S2), where each concentration was prepared in triplicate. The average recovery for each concentration was within 100.25 ± 0.92%, indicating a satisfactory accuracy. The % RSD for the nine preparations (three at each level) was found to be ≤2.0%, indicating acceptable precision of the method. The intermediate precision was investigated by the determination of LUH over 3 consecutive days. The % RSD for the intermediate precision is shown in (Table S2). The low % RSD indicates a satisfactory precision of the developed method.

The stability of the fabricated sensors was evaluated over a prolonged shelf life storage period through recording of the square-wave voltammograms at a fixed LUH concentration. Within the first month, the peak height remained constant (96.0% of the primary peak heights), which was diminished to about 92.5 and 89.2% after 30 and 60 days, respectively (Figure S6). The fabricated sensors showed high reproducibility measurements of the peak current and peak potential. The fabricated sensors are disposable, and the same electrode can be used for more than seven successive measurements without diminishing its performance of the peak height with an average recovery of 100 ± 1.09% (Figure S7).

3.7. Specificity (Interference Studies). To test the interference of various LUH degradation products, SWV was carried out for LUH at the optimal measuring conditions in an authentic mixture containing its alkaline, acidic, and oxidative degradants. No obvious interferences were recorded in the

https://doi.org/10.1021/acsomega.3c00040
ACS Omega 2023, 8, 10449−10458

existence of the aforementioned degradation products (Figure S8); therefore, it is possible to identify LUH among the corresponding degradants, and the proposed analysis protocol can be introduced as a stability-indicating approach.

The impact of the excipients and additives present in Latuda tablet (croscarmellose sodium and magnesium stearate, glucose, starch, citric acid, and propylene glycol) was examined through conducting SWV for 0.5 μg mL^{-1} of LUH in the absence and the presence of such interferents. The recorded average recoveries were acceptable, ranging from 95.96 ± 0.69 to 98.42 ± 0.35%, demonstrating the premium specificity of the introduced sensor.

3.8. Analytical Applications. To estimate the applicability of the SWV procedure for the identification and quantification of LUH, the presented method was applied for LUH content in a marketed Latuda 40 mg tablet in comparison to the reported HPLC method.[50] The results agreed effectively with the nominal content, and a standard addition scheme was implemented as shown in Table 2, which indicates values of the *t*-test and *F*-test less than the tabulated critical values.

Table 2. Statistical Analysis of Outcomes as per the Plot (SWV) for LUH at FeONPs/rGO Printed Sensors Compared With the Chromatographic Techniques[a]

parameters	(SWV)	reported HPLC method[65]
mean[a]	100.044	100.032
SD	0.10	0.11
variance	0.01258	0.01037
N	5	5
student's *t*-test (1.860)	0.431	
F-test (6.39)	1.213	

[a]Mean of five measurements, values in parentheses are the theoretical values corresponding to *t* and *F* at *P* = 0.05.

Additionally, the bio-analytical validation was verified, including the accuracy and precision of the proposed voltammetric measurement method in spiked urine. In drug-free urine samples, as explained before in the experimental section, no peak was observed at the predetermined potential of LUH. Then, the spiking of urine samples was elevated with predetermined concentrations of LUH, and the quantity of LUH recovered was determined. Statistical analysis of the data obtained was performed to test the reliability of the results and is displayed in Table 3.

Table 3. Estimation of the Precision and Accuracy of the SWV Technique for Quantification of LUH in Spiked Urine Samples at FeONPs/rGO Printed Sensors

parameters	sample 1	sample 2
added μg mL^{-1}	0.5	1.2
found[a]	0.502	1.195
recovery %	100.4	99.58
bias (%)	0.002	0.005
ref. method[70] (% found)	99.70	99.50
SD	0.114	0.272
RSD %	0.62	0.84
SE	0.120	0.087

[a]SD = standard deviation; RSD = relative standard deviation, SE = standard error. Mean of five measurements.

3.9. Green Chemistry Assessment. The prepared inkjet and procedures applied in the electroanalytical measurements were assessed in terms of environmental risks, suitability, and reliability for the environment using a semi-quantitative environmental analytical scale as an evaluation scale.[70,71] The systematic environmental scale is built on penalty points for demonstrated chemical hazards, potential exposure to occupational hazards, energy consumed by electrical devices, and waste-treatment methods; these are recorded by subtraction of the determined penalty points from 100 as an assessment metric. If the result is >50, green analysis is considered acceptable (Table S3). The overall penalty score for the proposed prepared inkjet and the voltammetric method was 65, indicating a suitable green analysis method.[72] The diminution in the score had been because of nanoparticle substances and printed substrate. We want to emphasize that some precautionary measures must be followed in order to minimize the risk of exposure, particularly for the analyst involved in the manufacturing and processing procedures. We want to assure that if certain preventive measures are followed, the risk of exposure, particularly to the analyst involved in handling and industrial procedures, is decreased.

4. CONCLUSIONS

The present work was devoted for the development of a novel printing ink matrix integrated with reduced graphene oxide and iron oxide nanostructures for the fabrication of flexible printed sensors. The surface morphological and electroanalytic features of the printed sensor were considered by using microscopic and voltammetric techniques, which indicates that the inkjet-printed sensor has good uniformity and stability and had no effect on the electrolyte solution. The constructed sensors were optimized and validated for sensitive and selective SWV determination of lurasidone in authentic samples in the presence of its degradants, spiked urine, and market pharmaceutical formulations. With an enhanced sensitivity, LUH molecule was oxidized at the electrode surface with a diffusion-controlled electrode reaction through the participation of two electrons/protons as assumed by the pH, scan rate, and molecular orbital calculation studies. At the optimum measuring conditions, LUH can be assayed within the linear concentration range from 0.050 to 2150 μg mL^{-1}, revealing an LOD value of 15.4 ng mL^{-1}. The fabricated sensor exhibited improved performance and can be introduced as an efficient tool for the sensitive and reliable voltammetric determination of LUH in pharmaceutical and biological samples. These results are expected to provide new insight into the effective sensing ability of our low-cost printed nanomaterials-based sensors that could provide a valuable tool for monitoring of pharmaceutical residues and drug-quality control.

■ ASSOCIATED CONTENT

Supporting Information

The Supporting Information is available free of charge at https://pubs.acs.org/doi/10.1021/acsomega.3c00040.

Photographs of the sample printed substrate for the FeONPs/rGO printed sensor and connector; cyclic voltammograms; molecular orbital model of lurasidone hydrochloride; HOMO structure of the LUH molecule; effect of voltage step potential on the anodic peak currents of LUH versus voltage step potential using the FeONPs/rGO printed sensor at pH 2.0; effect of pulse

https://doi.org/10.1021/acsomega.3c00040
ACS Omega 2023, 8, 10449−10458

amplitude on the anodic peak currents of LUH versus pulse amplitude using the FeONPs/rGO printed sensor at pH 2.0; intra- and inter-day precision and recovery data for SWV determination of LUH at the rGO/FeO/Gr sensor; and penalty points of the SWV method (PDF)

AUTHOR INFORMATION

Corresponding Authors

Mohammed A. Hussein − *Biochemistry Department, Faculty of Applied Medical Sciences, October 6 University, Giza 28125, Egypt*; orcid.org/0000-0002-1811-2794; Email: mhassan2372@gmail.com

Nashwa M. El-Metwaly − *Department of Chemistry, Faculty of Science, Mansoura University, Mansoura 35516, Egypt*; orcid.org/0000-0002-0619-6206; Email: nmmohamed@uqu.edu.sa, n_elmetwaly00@yahoo.com

Authors

Samar Y. Al-nami − *Department of Chemistry, Faculty of Science, King Khalid University, Abha 61421, Saudi Arabia*

Ali Q. Alorabi − *Department of Chemistry, Faculty of Sciences, Albaha University, Albaha 65799, Saudi Arbia*

Zehbah A. Al-Ahmed − *Depertment of Chemistry, College of Sciences and Art, Dhahran Aljounb, King Khalid University, Abha 61421, Saudi Arabia*

Amal T. Mogharbel − *Department of Chemistry, Faculty of Science, University of Tabuk, Tabuk 71474, Saudi Arabia*

Hana M. Abumelha − *Department of Chemistry, College of Science, Princess Nourah Bint Abdulrahman University, Riyadh 11671, Saudi Arabia*

Complete contact information is available at: https://pubs.acs.org/10.1021/acsomega.3c00040

Notes

The authors declare no competing financial interest.

All data generated or analyzed during this study are included in this published article (and its Supporting Information).

ACKNOWLEDGMENTS

The authors wish to acknowledge Princess Nourah bint Abdulrahman University Researchers Supporting Project number (PNURSP2023R22), Princess Nourah bint Abdulrahman University, Riyadh, Saudi Arabia.

REFERENCES

(1) Greenberg, W. M.; Citrome, L. Pharmacokinetics and pharmacodynamics of lurasidone hydrochloride, a second-generation antipsychotic: a systematic review of the published literature. *Clin. Pharmacokinet.* **2017**, *56*, 493−503.

(2) Lee, K. R.; Chae, Y. J.; Koo, T. S. Pharmacokinetics of lurasidone, a novel atypical anti-psychotic drug, in rats. *Xenobiotica* **2011**, *41*, 1100−1107.

(3) Jaeschke, R. R.; Sowa-Kućma, M.; Pańczyszyn-Trzewik, P.; Misztak, P.; Styczeń, K.; Datka, W. Lurasidone: The update on the pharmacology, efficacy and safety profile. *Pharmacol. Rep.* **2016**, *68*, 748−755.

(4) Franklin, R.; Zorowitz, S.; Corse, A. K.; Widge, A. S.; Deckersbach, T. Lurasidone for the treatment of bipolar depression: an evidence-based review. *Neuropsychiatr. Dis. Treat.* **2015**, *11*, 2143.

(5) Cruz, M. P. Lurasidone HCl (Latuda), an oral, once-daily atypical antipsychotic agent for the treatment of patients with schizophrenia. *Pharm. Therapeut.* **2011**, *36*, 489.

(6) Andrawis, M.; Ellison, L. C.; Riddle, S.; Mahan, K.; Collins, C. D.; Brummond, P.; Carmichael, J. Recommended quality measures for health-system pharmacy: 2019 update from the Pharmacy Accountability Measures Work Group. *Am. J. Health-Syst. Pharm.* **2019**, *76*, 874−887.

(7) Miao, Y.; Sun, J.; Chen, G.; Lili, R.; Ouyang, P. Enhanced oral bioavailability of lurasidone by self-nanoemulsifying drug delivery system in fasted state. *Drug Dev. Ind. Pharm.* **2016**, *42*, 1234−1240.

(8) Sharma, S.; Bhatt, S.; Saini, V. Formulation development and Evaluation of novel vesicular carrier for enhancement of bioavailability of poorly soluble drug. *Pharm. Nanotechnol.* **2021**, *9*, 70−82.

(9) Khan, Z. G.; Bari, S. B.; Patil, D. D. Lurasidone: A Review of analytical methods for Estimation in Pharmaceutical formulation. *Int. J. Life Sci. Rev.* **2016**, *2*, 17−22.

(10) Sri, K. V.; Sravani, S.; Kumar, M. S. Development and validation of UV spectrophotometric method for estimation of Lurasidone in bulk and pharmaceutical formulations. *Asian J. Pharm. Res.* **2015**, *5*, 102−107.

(11) Sudhir, M. S.; Nadh, R. V.; Manjunatha, H. Oxidative Coupling Reaction for the Determination of Lurasidone. *J. Anal. Chem.* **2019**, *74*, 528−533.

(12) Koo, T. S.; Kim, S. J.; Lee, J.; Ha, D. J.; Baek, M.; Moon, H. Quantification of lurasidone, an atypical antipsychotic drug, in rat plasma with high-performance liquid chromatography with tandem mass spectrometry. *Biomed. Chromatogr.* **2011**, *25*, 1389−1394.

(13) Katteboina, M. Y.; Pilli, N. R.; Mullangi, R.; Seelam, R. R.; Satla, S. R. LC-MS/MS assay for the determination of lurasidone and its active metabolite, ID-14283 in human plasma and its application to a clinical pharmacokinetic study. *Biomed. Chromatogr.* **2016**, *30*, 1065−1074.

(14) Damodar, K.; Bhogineni, S.; Ramanjaneyulu, B. RP-HPLC Method Development and Validation for the Analyisis of Lurasidone in Pharmaceutical Dosage Forms. *Drug Invent. Today* **2011**, *3*, 305−308.

(15) Kachave, R. N.; Mandlik, P. B.; Nisal, S. R. Liquid Chromatography Method Development and Validation of Related Impurities of Lurasidone and its Formulation. *Indian Drugs* **2018**, *55*, 41−48.

(16) Polawar, A. R.; Damle, M. C. Development and Validation of Stability Indicating hptlc Method for Quantification of Lurasidone HCl. *Pharma Sci. Monit.* **2014**, *5*, 131−144.

(17) McMaster, M. C. *HPLC: a Practical User's Guide*; John Wiley & Sons, 2007.

(18) Siddiqui, M. R.; AlOthman, Z. A.; Rahman, N. Analytical techniques in pharmaceutical analysis: A review. *Arab. J. Chem.* **2017**, *10*, S1409−S1421.

(19) Ozkan, S. A. *Electroanalytical Methods in Pharmaceutical Analysis and their Validation*; HNB publishing, 2012.

(20) Ozkan, S. A.; Kauffmann, J. M.; Zuman, P. *Electroanalysis in Biomedical and Pharmaceutical Sciences: Voltammetry, Amperometry, Biosensors, Applications*; Springer, 2015.

(21) Ziyatdinova, G.; Budnikov, H. Electroanalysis of antioxidants in pharmaceutical dosage forms: state-of-the-art and perspectives. *Monatsh. Chem.* **2015**, *146*, 741−753.

(22) Cavalheiro, É.T. G.; Brett, C.; Oliveira-Brett, A. M.; Fatibello-Filho, O. Bioelectroanalysis of pharmaceutical compounds. *Bioanal. Rev.* **2012**, *4*, 31−53.

(23) Bitew, Z.; Amare, M. Recent reports on electrochemical determination of selected antibiotics in pharmaceutical formulations: a mini review. *Electrochem. Commun.* **2020**, *121*, 106863.

(24) Michalkiewicz, S.; Skorupa, A.; Jakubczyk, M. Carbon Materials in Electroanalysis of Preservatives: A Review. *Materials* **2021**, *14*, 7630.

(25) Ghalkhani, M.; Ghorbani-Bidkorbeh, F. Development of carbon nanostructured based electrochemical sensors for pharmaceutical analysis. *Iran. J. Pharm. Res.* **2019**, *18*, 658.

(26) Althagafi, I. I.; Ahmed, S. A.; El-Said, W. A. Fabrication of gold/graphene nanostructures modified ITO electrode as highly sensitive electrochemical detection of Aflatoxin B1. *PLoS One* **2019**, *14*, No. e0210652.
(27) Shawky, A. M.; El-Tohamy, M. F. Highly functionalized modified metal oxides polymeric sensors for potentiometric determination of letrozole in commercial oral tablets and biosamples. *Polymers* **2021**, *13*, 1384.
(28) Elmosallamy, M. A.; Saber, A. L. Recognition and quantification of some monoamines neurotransmitters. *Electroanal* **2016**, *28*, 2500−2505.
(29) Kassem, M. A.; Hazazi, O. A.; Ohsaka, T.; Awad, M. I. Electroanalysis of pyridoxine at copper nanoparticles modified polycrystalline gold electrode. *Electroanal* **2016**, *28*, 539−545.
(30) Al-Qahtani, S. D.; Hameed, A.; Alamrani, N. A.; Alharbi, A.; Shah, R.; Al-Ahmed, Z. A.; El-Metwaly, N. M. Zinc Oxide Nanostructured-Based Sensors for Anodic Stripping Voltammetric Determination of Darifenacin. *J. Electrochem. Soc.* **2022**, *169*, 066512.
(31) Moya, A.; Gabriel, G.; Villa, R.; Javier del Campo, F. J. Inkjet-printed electrochemical sensors. *Curr. Opin. Electrochem.* **2017**, *3*, 29−39.
(32) Kamarudin, S. F.; Mustapha, M.; Kim, J. K. Green strategies to printed sensors for healthcare applications. *Polym. Rev.* **2021**, *61*, 116−156.
(33) Maddipatla, D.; Narakathu, B. B.; Atashbar, M. Recent progress in manufacturing techniques of printed and flexible sensors: a review. *Biosensors* **2020**, *10*, 199.
(34) Beitollahi, H.; Mohammadi, S. Z.; Safaei, M.; Tajik, S. Applications of electrochemical sensors and biosensors based on modified screen-printed electrodes: a review. *Anal. Methods* **2020**, *12*, 1547−1560.
(35) Liu, H.; Zhang, H.; Han, W.; Lin, H.; Li, R.; Zhu, J.; Huang, W. 3D printed flexible strain sensors: from printing to devices and signals. *Adv. Mat.* **2021**, *33*, 2004782.
(36) Tyszczuk-Rotko, K.; Kozak, J.; Czech, B. Screen-printed voltammetric sensors—Tools for environmental water monitoring of painkillers. *Sensors* **2020**, *22*, 2437.
(37) Ferrari, A. G.-M.; Rowley-Neale, S. J.; Banks, C. E. Screen-printed electrodes: Transitioning the laboratory in-to-the field. *Talanta* **2021**, *3*, 100032.
(38) dos Santos, D. M.; Cardoso, R. M.; Migliorini, F. L.; Facure, M. H.; Mercante, L. A.; Mattoso, L. H.; Correa, D. S. Advances in 3D printed sensors for food analysis. *TrAC, Trends Anal. Chem.* **2022**, *154*, 116672.
(39) Bounegru, A. V.; Apetrei, C. Carbonaceous nanomaterials employed in the development of electrochemical sensors based on screen-printing technique—A review. *Catalysts* **2020**, *10*, 680.
(40) Ambaye, A. D.; Kefeni, K. K.; Mishra, S. B.; Nxumalo, E. N.; Ntsendwana, B. Recent developments in nanotechnology-based printing electrode systems for electrochemical sensors. *Talanta* **2021**, *225*, 121951.
(41) Sharma, D.; Hussain, C. M. Smart nanomaterials in pharmaceutical analysis. *Arab. J. Chem.* **2020**, *13*, 3319−3343.
(42) Qian, L.; Durairaj, S.; Prins, S.; Chen, A. Nanomaterial-based electrochemical sensors and biosensors for the detection of pharmaceutical compounds. *Biosens. Bioelectron.* **2021**, *175*, 112836.
(43) Agnihotri, A. S.; Varghese, A.; M, M. Transition metal oxides in electrochemical and bio sensing: A state-of-art review. *Appl. Surf. Sci. Adv.* **2021**, *4*, 100072.
(44) Buledi, J. A.; Shah, Z. U. H.; Mallah, A.; Solangi, A. R. Current perspective and developments in electrochemical sensors modified with nanomaterials for environmental and pharmaceutical analysis. *Curr. Anal. Chem.* **2022**, *18*, 102−115.
(45) Urbanova, V.; Magro, M.; Gedanken, A.; Baratella, D.; Vianello, F.; Zboril, R. Nanocrystalline iron oxides, composites, and related materials as a platform for electrochemical, magnetic, and chemical biosensors. *Chem. Mater.* **2014**, *26*, 6653−6673.
(46) Cp, K. P.; Aralekallu, S.; Sajjan, V. A.; Palanna, M.; Kumar, S.; Sannegowda, L. K. Non-precious cobalt phthalocyanine-embedded iron ore electrocatalysts for hydrogen evolution reactions. *Sustain. Energy Fuels* **2021**, *5*, 1448−1457.
(47) Nemakal, M.; Shantharaja, M.; Giddaerappa, L. K.; Palanna, P. S.; Koodlur Sannegowda, L.; Sharath Kumar, P. Zinc phthalocyanine anchored magnetite particles: Efficient platform for sensing of thiocyanate. *J. Electroanal. Chem.* **2021**, *895*, 115385.
(48) Al-Qahtani, S. D.; Hameed, A.; Aljuhani, E.; Shah, R.; Alharbi, A.; Asghar, B. H.; El-Metwaly, N. M. Iron oxide nanopowder based electrochemical sensor for sensitive voltammetric quantification of midodrine. *Arab. J. Chem.* **2021**, *14*, 103446.
(49) Khalilzadeh, M. A.; Tajik, S.; Beitollahi, H.; Venditti, R. A. Green synthesis of magnetic nanocomposite with iron oxide deposited on cellulose nanocrystals with copper (Fe3O4@ CNC/Cu): investigation of catalytic activity for the development of a venlafaxine electrochemical sensor. *Ind. Eng. Chem. Res.* **2020**, *59*, 4219−4228.
(50) Suneetha, A.; Manasa, K.; Lakshmi Sindhura, S. L. Stability indicating RP-HPLC method for determination and validation of lurasidone HCL in bulk and pharmaceutical dosage forms. *J. Pharm. Res.* **2015**, *14*, 15−19.
(51) Jouikov, V.; Simonet, J. Electrochemical reactions of sulfur organic compounds. In *Encyclopedia of Electrochemistry*; Bard, A. J., Stratmann, M., Scholz, F., et al, Eds.; Wiley-VCH Verlag GmbH & Co: Weinheim, Germany, 2007; Vol. *8*.
(52) Mersal, G. A. Electrochemical applications and computational studies on ephedrine drug. *J. Solid State Electrochem.* **2012**, *16*, 2031−2039.
(53) Zhang, L.; Li, Y.; Zhang, L.; Li, D. W.; Karpuzov, D.; Long, Y. T. Electrocatalytic oxidation of NADH on graphene oxide and reduced graphene oxide modified screen-printed electrode. *Int. J. Electrochem. Sci.* **2011**, *6*, 819−829.
(54) Rebelo, P.; Pacheco, J. G.; Cordeiro, M. N. D.; Melo, A.; Delerue-Matos, C. Azithromycin electrochemical detection using a molecularly imprinted polymer prepared on a disposable screen-printed electrode. *Anal. Methods* **2020**, *12*, 1486−1494.
(55) Wang, J.; Pedrero, M.; Sakslund, H.; Hammerich, O.; Pingarron, J. Electrochemical activation of screen-printed carbon strips. *Analyst* **1996**, *121*, 345−350.
(56) Elancheziyan, M.; Ganesan, S.; Theyagarajan, K.; Duraisamy, M.; Thenmozhi, K.; Weng, C. H.; Lin, Y. T.; Ponnusamy, V. K. Novel biomass-derived porous-graphitic carbon coated iron oxide nanocomposite as an efficient electrocatalyst for the sensitive detection of rutin (vitamin P) in food and environmental samples. *Environ. Res.* **2022**, *211*, 113012.
(57) Motia, S.; Bouchikhi, B.; Llobet, E.; El Bari, N. Synthesis and characterization of a highly sensitive and selective electrochemical sensor based on molecularly imprinted polymer with gold nanoparticles modified screen-printed electrode for glycerol determination in wastewater. *Talanta* **2020**, *216*, 120953.
(58) Fanjul-Bolado, P.; Hernández-Santos, D.; Lamas-Ardisana, P. J.; Martín-Pernía, A.; Costa-García, A. Electrochemical characterization of screen-printed and conventional carbon paste electrodes. *Electrochim. Acta* **2008**, *53*, 3635−3642.
(59) Ngamchuea, K.; Eloul, S.; Tschulik, K.; Compton, R. G. Planar diffusion to macro disc electrodes—what electrode size is required for the Cottrell and Randles-Sevcik equations to apply quantitatively. *J. Solid State Electrochem.* **2014**, *18*, 3251−3257.
(60) Qian, S.; Heng, W.; Wei, Y.; Zhang, J.; Gao, Y. Coamorphous lurasidone hydrochloride−saccharin with charge-assisted hydrogen bonding interaction shows improved physical stability and enhanced dissolution with pH-independent solubility behavior. *Cryst. Growth Des.* **2015**, *15*, 2920−2928.
(61) Stanković, D.; Mehmeti, E.; Svorc, L.; Kalcher, K. New electrochemical method for the determination of β-carboline alkaloids, harmalol and harmine, in human urine samples and in Banisteriopsis caapi. *Microchem. J.* **2015**, *118*, 95−100.
(62) Zhang, Z.; Wang, E. *Electrochemical Principles and Methods*; Science Press: Beijing, 2000.
(63) Gosser, D. K. *Cyclic Voltammetry, Simulation and Analysis of Reaction Mechanisms*; Wiley VCH: New York, 1993.

https://doi.org/10.1021/acsomega.3c00040
ACS Omega 2023, 8, 10449−10458

(64) Laviron, E. Adsorption, autoinhibition and autocatalysis in polarography and in linear potential sweep voltammetry. *J. Electroanal. Chem.* **1974**, *52*, 355−393.
(65) Elgrishi, N.; Rountree, K. J.; McCarthy, B. D.; Rountree, E. S.; Eisenhart, T. T.; Dempsey, J. L. A practical beginner's guide to cyclic voltammetry. *J. Chem. Educ.* **2018**, *95*, 197−206.
(66) Laviron, E. Theoretical study of a reversible reaction followed by a chemical reaction in thin layer linear potential sweep voltammetry. *J. Electroanal. Chem. Interfacial Electrochem.* **1972**, *39*, 1.
(67) Nicholson, R. S. Theory and application of cyclic voltammetry for measurement of electrode reaction kinetics. *Anal. Chem.* **1965**, *37*, 1351−1355.
(68) Caccia, S.; Pasina, L.; Nobili, A. Critical appraisal of lurasidone in the management of schizophrenia. *Neuropsychiatr. Dis. Treat.* **2012**, *8*, 155.
(69) Walfish, S. Analytical methods: a statistical perspective on the ICH Q2A and Q2B guidelines for validation of analytical methods. *BioPharm. Int.* **2006**, *19*, 40.
(70) Gałuszka, A.; Migaszewski, Z. M.; Konieczka, P.; Namieśnik, J. Analytical Eco-Scale for assessing the greenness of analytical procedures. *TrAC, Trends Anal. Chem.* **2012**, *37*, 61−72.
(71) Tobiszewski, M.; Marć, M.; Gałuszka, A.; Namieśnik, J. Green chemistry metrics with special reference to green analytical chemistry. *Molecules* **2015**, *20*, 10928−10946.
(72) Serrano-Luján, L.; Víctor-Román, S.; Toledo, C.; Sanahuja-Parejo, O.; Mansour, A. E.; Abad, J.; Amassian, A.; Benito, A. M.; Maser, W. K.; Urbina, A. Environmental impact of the production of graphene oxide and reduced graphene oxide. *SN Appl. Sci.* **2019**, *1*, 179.

https://doi.org/10.1021/acsomega.3c00040
ACS Omega 2023, 8, 10449−10458